In Silico Studies and Design of Scrupulous Novel Sensor for Nitro Aromatics Compounds and Metal Ions Detection

Ajay L Desai
Ganpat University
Nihal P Patel
Ganpat University
Jaymin H Parikh
Ganpat University
Krunal M Modi
Ganpat University
Keyur D Bhatt (drkdbhatt@outlook.com)
Ganpat University https://orcid.org/0000-0001-9301-576X

Research Article

Keywords: calix[4]pyrrole, nitro-aromatic compounds, metal ions, sensing, host-guest interaction, fluorescence, in-silico studies

Posted Date: October 22nd, 2021

DOI: https://doi.org/10.21203/rs.3.rs-914744/v1

Version of Record: A version of this preprint was published at Journal of Fluorescence on January 4th, 2022. See the published version at https://doi.org/10.1007/s10895-021-02866-2.

In silico studies and design of scrupulous novel sensor for nitro aromatics compounds and metal ions detection

Ajay L. Desai, Nihal P. Patel, Jaymin H. Parikh, Krunal M. Modi*, Keyur D. Bhatt*

Department of Chemistry, Mehsana Urban Institute of Sciences, Ganpat University, Kherva, Gujarat, 384012, India

Abstract

A Novel Calix[4]pyrrole system bearing carboxylic acid functionality [ABuCP] has been synthesized and its interaction towards various nitroaromatics compounds [NACs] were investigated. ABuCP showed significant color change with 1,3-dinitro benzene (1,3-DNB) in comparison to the solution of other nitroaromatic compounds such as 2,3-dinitro toluene (2,3-DNT), 2,4-dinitro toluene (2,4-DNT), 2,6-dinitro toluene (2,6-DNT), 4-NBB (4-nitrobenzyl bromide) and 4-nitro toluene (4-NT). The ABuCP-1,3-DNB complex produces a red shift in absorption spectra based on charge transfer mediated recognition. Additionally, the density functional theory calculation confirmed the possible mechanism for the binding of 1,3-DNB as a guest is well supported by the calculation of other parameters such as hardness, stabilization energy, softness, electrophilicity index and chemical potential. The TDDFT calculation facilitates the understanding of the proper binding mechanism in reference to experimental results. Additionally we have also developed its derivative which acts as a new fluorescent sensor which can selectively recognize Sr(II) ion. In this view its aminoanthraquinone derivative of calix[4]pyrrole i.e. ABuCPTAA is synthesized which also results in generation of high fluorescence capability sensor.

Keywords: calix[4]pyrrole; nitro-aromatic compounds; metal ions, sensing, host-guest interaction, fluorescence, in-silico studies.

Corresponding mail ID: drkdbhatt@outlook.com

1.0. Introduction

Nitroaromatics (NACs: hazardous electrophilic species) in the conspicuous matter in this century because of its harmfulness to human health and environment. The production, Storage abuse of this nitro aromatic compounds mainly their uses in terrorist and war activity pose great to public security of the whole world [2-5]. As one kind of important pollutions, NACs such as trinitrophenol, nitrophenol, dinitrobenzene and trinitrotoluene also cause health problems in both animals and human beings, including anaemia, abnormal liver function, cataract development and skin irritation [6,7]. Even after degradations, the by-products of the common nitro aromatic compounds are still potent carcinogenic and due to this they are referred as priority pollutants [8,9]. Some di-nitroaromatics, especially m-dinitrobenzene (m-DNB) finds application in industry as an intermediate in the chemical synthesis of some rubber chemical, pesticides, dyes, and nitro aromatic compounds [10] and they have been detected also in groundwater near industrial waste disposal sites [2]. Compared with other nitroaromatic compounds, m-DNB could cause methemoglobinemia in animals and humans [11]. It could also produce testicular toxicity [12], and brainstem damage [10,11]. Abundant papers have been published on the identification and quantification of nitro aromatic compounds. At present, numerous kinds of modern instruments such as GCMS, LCMS, Ion mobility spectroscopy, fluorescence, X-ray dispersion, Raman spectroscopy and chemiluminescence [13-16] are being engaged for the sensitive and selective sensing of NAC, but usually are torment from the disadvantages like high operational cost and portability units during in-field use, and this has limited production of small, low-power units suitable for use in the field which greatly limits their extensive application. But for the same if a molecular sensor is designed and synthesized such that it will be sensitive to our m-DNB that produces a visible optical change in the presence of nitro aromatic compounds even at very low concentration under rather elementary conditions. Such systems, which rely on changes in absorption, can be employed in the absence of instrumentation via simple “naked eye” detection. They can also be incorporated as faster, cheaper, and safer analysis.

In this view, calixarene based chemosensors have been reported to exhibit unique response towards any analyte of curiosity based on the optimized structural as well as geometrical factors [17-19]. Modification of calixarene structures can be made to detect nitro aromatic compounds in its ingredient solutions [20-22]. Nowadays, pyrrole-based macrocycles are on the forefront for the development of such selective receptors. Calix[4]pyrrole and its

substituents derivatives holds a great perspective in the fields of sensors [23-26], and their distinctive behaviors attributed due to its structural flexibility [27,28]. It is well-known that non-covalent interaction such as hydrophobic effects, pi-pi stacking, van der Waals forces, Hydrogen bonding, metal coordination, cation-pi interactions, are responsible for the function of synthetic or natural supramolecular in biological processes, such as immune response, protein enzyme inhibitors, signal transduction or normal function of cellular/organelle structure [29-31]. One of the approaches which would fit our detection of nitro aromatic compounds involves charge transfer (CT) donor-acceptor complexes [32-34]. For the same, our present study is to signify the neutral molecular recognition ability of calix[4]pyrrole tetracarboxylic acid (ABuCP) ligands. Over the last decade, our group has synthesized several calix based chemosensors [35-37,5] but this application can be either an extension to our effort to build up a sensor for NACs. Our goal was to use optical and more specifically colorimetric means of signalling to selectively detect nitro aromatic compounds with low concentration limits and ABuCP serves as an excellent colorimetric sensor. Moreover, the In-silico insights could provide a theoretical as well as preparative chemistry towards host-guest interaction of ABuCP and 1,3 DNB.

Additionally, several advanced analytical methods are available today for the identification and quantification of ions and molecules of environmental importance. The most prominent techniques involving metal ion and anion recognition include atomic absorption spectroscopy (AAS), ICP-OES, ICP-MS, Ion chromatographic imagery (IC), X-ray fluorescence spectroscopy (ICP-MS), induced plasma mass spectroscopy (ICP-MS) (XRF). In addition to these approaches, some electroanalytical techniques like as potentiometry amperometry, some electroanalytical techniques like as potentiometry, amperometry and cyclic voltammetry are often employed for the identification of different guest analytes, These processes include costly tools, skilled personal and arduous preparatory techniques for the sample to get extremely accurate findings. The chromogenic sensors [38-42] are thus the main prerequisite for one-site analytics detection. Active field of study is the detection of fluorescence of chemical and biological analytes. The aim of such initiatives is to reduce the costly usage and disposal of radioactive tracers. Fast and cost-effective diagnostic techniques for a variety of clinic, bioprocess and environmental applications are also required. In general, Fluorometry is regarded preferable to spectrophotometry since it is particularly more sensitive. Techniques of fluorescence can measure correctly up to one million times lower concentration than measures

of absorbance. Furthermore, via time-resolved measurements, analyte distinguishing ability is higher.

So, our view is to develop a new fluorescent sensor which can selectively recognize cations. In an attempt to execute our vision aminoanthraquinone derivatives [25] of calix[4]pyrrole i.e. **ABuCPTAA** is synthesized which will result in generation of high fluorescence capability sensors.

2. Materials and Methods

2.1. Chemical and materials

All metals salts, nitroaromaic compounds (NACs), and ingredients, such as 8-, 1-aminoanthraquinone, 4-acetylbutyric acid and pyrrole were obtained from Sigma-Aldrich, while additional solvents and reagents were obtained from commercial sources. Merck provided TLC plates with fluorescence active (F-254). Magnetic stirrer (REMI-5MLH) and micro-pipette (VAR VOL 100-1000 µl, Kasablanka-Mumbai) were used. All the glassware was very well calibrated before use.

2.2. Instruments

The melting points (uncorrected) were obtained from a VEGO model; VMP-DS, (Mumbai, India). Samples for infrared spectra were prepared as KBr pallets; spectra were recorded on tensor Bruker 27 (IISER, Pune) and expressed in cm^{-1}. Elemental analysis (C, H, and N) was performed on vario MICRO-Variant elemental analyzer (Mt. Laurel, USA). Electrospray ionization (ESI) mass spectra (MS) were determined using micromassQuarter2 (CSMCRI, Bhavnagar). NMR spectra were recorded on a model DPX 200 MHz and Avance II 400 MHz Bruker FT-NMR instrument (Ettlingen, Germany). Microwave irradiation was carried out in Samsung MC28H5025VS/TL (Ganpat University, Gujarat), while UV-Vis spectra were recorded on a SCHIMADZU-1900 spectrophotometer (MUIS, Ganpat University). Fluorescence spectra were obtained on a Jasco spectrofluorimeter FP 8300 (xenon lamp headxe90) spectrometer (Department of Chemistry, Gujarat University, Gujarat).

2.3. General method for spectroscopic detection of nitro aromatic compounds and cations

Absorption spectra of **ABuCP** stock solution (2×10^{-5} M) and those of various nitroarmatic compounds (2×10^{-5} M) with 100 equivalents were prepared in MeOH solvent and were

recorded and compared. Absorption spectra of resulting solution mixture of same stock solution of ligand were used and nitro aromatic compounds solutions of pet concentration (1.0-100 equiv.) were prepared by dilution of stock solution.

Emission spectra were recorded using **ABuCPTAA** stock solution ($2x10^{-5}$ M) and different desired concentration (1.0 – 100 equivalents) of corresponding cations (2×10^{-5} M) such as Mg (II), Co (II), Ni (II), Cd (II), Pb (II), Sr (II), Cu (II), Bi (II), Cr (II) and Al (II) were taken by fitting dilution with same stock solution. Spectra were recorded and compared. The binding constant of the complex was also established using the method described in the literature. Here the interaction of Sr (II) with ligand ABuCPTAA is studied.

2.4. Computational methodology

2.4.1. Density Functional Theory Calculation:

The Density Functional theory calculation have been performed using Hartree-Fock (HF), Becke's three-parameter hybrid exchange (B3LYP) and Coulomb-attenuating method-Becke's three-parameter hybrid exchange (CAM-B3LYP) [43] in the Gaussian 09 (G09 B.01) software package [44,45]. The geometric structures of the complex have been fully optimized at HF, B3LYP and CAM-B3LYP levels as well as 6-31g(d,p), 6-31g++(d,p) in the ground state (singlet). The ABCPs were demonstrated using Avogadro version 1.2.0 software [46]. The conductor-like polarizable Continuum Model (CPCM) has been systematically monitored for all the steps for the effect of solvent (methanol). The Highest occupied molecular orbital (HOMO) and lowest unoccupied molecular orbital (LUMO), electron density (ED), electrostatic potential (ESP), and Molecular electrostatic potential (MEP) was performed at Cam-B3LYP method with 6-31G(d,p) basis sets.

2.4.2. Host-Guest Interaction:

The molecular level interaction of selective nitro aromatic compounds was employed in the glide module of the Maestro suite of Schrodinger software [47,48]. Glide extra precision (XP) was applied for the molecular docking which includes the false positive rates that are removed by more thorough screening and enhanced scoring, resulting in much greater enrichment. The receptor grid was generated using the grid generation wizard in Glide to build a three-dimensional (3D) grid with a maximum scale of 20x20x20 and 0.5 spacing. Ligand preparation has been performed using the Ligprep Module [49]. After that the binding affinity and interactions were examined.

2.5. *4,4',4'',4'''-(5,10,15,20-tetramethyl-5H,10H,15H,20H,22H,24H-porphyrin-5,10,15,20-tetrayl)tetrabutyric acid (ABuCP) via conventional and microwave methods:*

2.5.1. Conventional method:

Parent 4-acetyl substituted calix[4]pyrrole skeleton **(Scheme 1)** was synthesized using general method of acid catalyzed condensation reaction of pyrrole and aliphatic acid. Distilled pyrrole (1.0 ml, 0.0153 mmol) was placed in a 250 ml round bottom flask equipped with magnetic stirrer and filled with acetonitrile (100 ml). Boron trifluoride etherate (2.11 ml) was then added to the reaction flask and stirred for 15 minutes. 4-acetyl butyric acid (2.00 ml, 0.0153 mmol) was dissolved in acetonitrile (100 ml) and added stepwise to the reaction flask. Reaction mixture was left to stir for 8 hours and was monitored through TLC. After completion of reaction, the reaction mixture was poured slowly into another 500 ml round bottom flask equipped with a magnetic stirrer and distilled water (200 ml) containing triethyl amine to obtain a light brown colored residue. It was filtered, collected, and dissolved in diethyl ether (400 ml) to get rid of the black tar. The solvent was evaporated to obtain light brown-black residue, which was then recrystallized from methanol to obtain pure product (58%).

2.5.2 Microwave irradiation:

A mixture of pyrrole (0.125 ml, 0.0018 mol) and boron trifluoride etherate (0.26 ml) in acetonitrile (10 ml) were exposed to microwave irradiation for 10 min. A solution of 4-acetylbutyric acid (0.3058 gm, 0.0018mol) in acetonitrile (10 ml) was then added to the reaction mixture and was subjected to microwave irradiation for 10 minutes with a slight pause after every 2 minutes. After completion of the reaction, a light brown-black reaction mixture was poured into cold water (50 ml) to obtain brown black colored precipitates. The residue was filtered off, collected, dried and dissolved in diethyl ether (25 ml x 2). The solution was again filtered gravitationally to get rid of the black tar. The solvent was evaporated to obtain light brown colored residue which was then recrystallized from a methanol mixture to get pure product for analysis.

2.5.3 *Synthesis of tetrakis(-(9,10-dioxo-4a,9,9a,10-tetrahydroanthracen-1-yl)amino)-2-oxoethyl)4,4',4'',4'''-(5,10,15,20-tetramethyl 5H,10H,15H,20H,22H,24H-porphyrin-5,10,15,15,20-tetrayl)tetrabutyrate: ABuCPTAA*

Step I: Synthesis of 2-chloro-N-(9,10-dioxo-9,10-dihydroanthracen-1-yl) acetamide

To the solution of 1-aminoanthraquinone (0.6g, 0.9 mmol) dissolved in $CHCl_3$ slow addition of 2-chloroacetyl chloride (0.83g, 3.7mmol) was carried out by stirring. This reaction mixture was further stirred for 2 hours and progress was monitored through TLC. After the completion of reaction the reaction mixture was washed with water and recrystallized from DCM to obtain 2-chloro-N-(9,10-dihydroanthracen-1-yl)acetamide [50,25].

Step II: Synthesis of calix[4]pyrrole-N-(9,10-dioxo-9,10-dihydroanthracen-1-yl) acetamide ***(ABuCPTAA)***

The reaction mixture containing ABuCP (0.4g, 0.000559mol), K_2CO_3 (0.31g, 0.00291mol), KI (catalytic amount) and 2-chloro-N-(9,10-dioxo-9,10-tetrahydroanthracen-1-yl)acetamide (0.67g, 0.002235mmol) in acetone was refluxed for 48 hours and progress of reaction mixture was monitored through TLC. After completion of reaction temperature was slowly brought down to room temperature and the solvent was removed by filtration. The fraction was separated, dried to give ABuCPTAA **(Scheme 2).**

3.0. Result and discussion

3.1. Absorption Spectra

Absorption spectroscopy has been utilized for the investigation of the overall binding property of 1,3- DNB with ligand ABuCP. The UV-visible absorption spectrum of the ABuCP a peak was observed at a wavelength of 210 nm. Absorption band shift from 210 to 234 nm with red shift of 24nm (**Figure 2**) was observed upon addition of 1,3-DNB, meanwhile no absorption spectrum change was observed when other nitro aromatic compounds were added. Also, variation of absorption intensity as well as wavelength upon the addition of gradually increasing concentration of 1,3-DNB was studied (**Figure 3**). A charge transfer between ABuCP and 1,3 – DNB occurs which is responsible for inducing shifting of the absorption band towards higher wavelength. Moreover, regarding the chemical potential it was found that, in the direction of pyrrole ring more +ve potential Is found and that the more negative potential is in the direction of carboxylic group of butyric acid as well as 1,3 – DNB compared to that ABuCP and 1,3-DNB, thus there are maximum possibilities of ABuCP to attract 1,3-DNB via hydrogen bonding as well as electrostatic interaction which is described later in in-silico studies. Interestingly, ABuCP-1,3-DNB complex forms a novel supramolecular recognition host system that can discriminate 1,3-DNB from other nitro aromatic compounds. It can be postulated that the synergistic effects of stacking and

electrostatic interaction and red shift induces selection colorimetric signals for the ABuCP in presence of other nitro aromatic compounds.

Also, investigation of ABuCPTAA as a fluorescent probe was very well studied by absorption (**Figure 4)** and emission spectra of ABuCPTAA with various metal ions: Mg (II), Co (II), Ni (II), Cd (II), Pb (II), Sr (II), Cu (II), Bi (II), Cr (II) and Al (II) as their nitrate salts were recorded in MeOH as solvent. Sr(II) ions was the only cation to show interaction with ABuCPTAA among other tested cations. Also variation of absorption intensity as well as wavelength upon the addition of gradually increasing concentration of Sr (II) ions was studied (**Figure 5**) .Emission spectra (**Figure 6**) showed a remarkable quenching of 80%, which indicates charge transfer mechanism. Carbonyl group on aminoanthraquinone acts as an excellent donor and experiences ICT [25,42,51]. Electron rich oxygen provides electron to electron deficient ring. This ICT mechanism [52] continues until Sr (II) is not added, the time when Sr (II) is added ICT decreases as the formation of a bond between carbonyl oxygen of anthraquinone group that was initially directly attached with anthraquinone ring. The charge transfer from the oxygen of the anthraquinone group to the electron deficient ring stops when the charge density on the oxygen atom decreases, resulting in a drop in emission intensity leading to quenching [25,50]. Also, Emission spectra were increased in respect to decrease in concentration Sr (II) ions **Figure 7.**

3.2. Stoichiometry of complex

Job's method [53] of continuous variation was employed for the determination of stoichiometry ratios of the metal ligand complex.

$$\Delta \mathbf{A} = \mathbf{A_c} - \mathbf{A_b} \qquad \textbf{(1)}$$

$\Delta \mathbf{A}$ values were plotted against mole fraction of Sr (II) ions a/a + b **(Figure 8).** The obtained value of 0.50 for ΔA at a/a + b indicates a 1:1 ratio single formation of complex. The precision of this result implies the formation of a single complex. To ensure its reliability the measurement was done at different wavelengths. This gave the same values for a/a + b ratio.

3.3. Binding Constant and quantum yield of ABuCPTAA

With a previously published procedure and given equation [23,54,55], the binding constant of fluoroionophore was established.

$$(F_O\text{-}F)/(F\text{-}F_1) = [M]/((K_{diss})^n \qquad (2)$$

Here guest concentration [M] scales with the fluorescence intensity F. Binding constant K_s is obtained by plotting of log [M] against log $[(F_0\text{-}F)/(F\text{-}F_1)]$, where F_0 is complex fluorescence intensities in absence of guest and F_1 is fluorescence intensity in presence of maximum concentration of guest. The value of the reciprocal of binding constant K_s i.e., log (K_{diss}) is obtained via plotting log [M] versus log $[(F_0 – F_1) / (F – F_1)]$. A good linear fit of R = 0.98 and 0.97 is obtained using the above equation for ABuCPTAA.

Fluorescence quantum yields *(ϕ_F)* [23] is obtained using following method.

$$\emptyset = \emptyset std \ \frac{FAStd\eta 2}{FStdA\eta 2Std} \qquad (3)$$

Emission curve of guest with ligand is illustrated by F and F_{std} indicates the standard curve of ligand. A_{std} is absorption wavelength and A is absorbance relative to the sample. Refractive index of MeOH used in standard. Same wavelength is used in excitation of both standard and sample. Approximately reported quantum yield of amino-anthraquinone is 0.075 and that of ABuCPTAA is obtained as 0.71 which is showing the occurrence of quenching phenomenon due to increased addition of guests resulting in decreasing the number of emitted photons **(Table 1).**

3.4. Colorimetric detection of 1,3-DNB using ABCP

Functionalized calix[4]pyrrole receptor, ABuCP bearing four separate acetyl-butyric substituents fused onto the β-pyrrolic position of the calix[4]pyrrole core, and showed that this system was able to bind 1,3-dinitro benzene (1,3-DNB) in 1:1 fashion. The binding of DNB is accompanied by an east-to-visualize change in color from light brown to dark brown, making this system of potential interest as a colorimetric sensor. The nitro aromatic compounds i.e 2,3-DNB, 2,4-DNT, 2,6-DNT, 4-NB, 1,3-DNB, and 4-NT in 1μM concentration were introduced to these ligands (ABuCP). No noticeable color change was detected by naked eye with. any of the nitro aromatic compounds except 1,3-DNB, which exhibited a change in color from light brown to dark brown **(Figure 9).** The color change with 1,3-DNB could easily be detected at even at nanomolar (nM) concentration in methanol solvent. We can inferred from this results that ligand ABuCP could serve as an efficient selective colorimetric sensor for 1,3-DNB [20,56,57].

Stability of ABCP has been investigated by change in their UV Visible spectrum intensity at different pH (4.0-11.0). UV-Visible band of ABuCP displays slight change at pH other than 7.0 – 8.0 and is liable to being some- what turbid. However, if it is exploited to sonicating process for 10-15 mins, they retain their ingenuity with insignificant compromise in their UV spectrum. Likewise. Their absorption intensity of ligand ABCP is slightly quenched at pH other than 7.0. Hence, pH 7.0 was preferred to carry out all experiments on ABuCP and determined that ligand shows maximum stability (**Figure 10**) with wavelength and absorption intensity at pH 7.0 also the same was showing good results at room temperature **(Figure 11 and Figure 12).**

3.5. In-silico Optimization:

The Ligand ABuCP as well as other Nitroaromatic nitro aromatic compounds (NACs) was optimized in gas as well as Solvent to get an insight of binding posture of the complex. **Table 2** represents the Optimization value Gas phase and Solvent phase.

3.6. Docking Interaction:

The molecular docking interaction has been performed using Schrodinger glide docking [47]. In the docking study, as an input structural the geometry optimized host structure (ABuCP) (**Figure 13**) and guest (All NACs) has been utilized. The highest glide docking energy play a crucial role for the establishment of the tunable and finest docking of ABuCP with all NACs (**Figure 14**)which advocate the stable complex formation between the ABuCP and 1,3-DNB having two different poses. **(Figure 15 and 16).** The energy of post 1 is -13.771 kcal/mol and Pose 2 is -13.389 kcal/mol which is higher than others. In the docking, mainly two types of interaction play crucial roles for the complex formation and docking energy.
One is noncovalent interaction (classical hydrogen bonding, and Aromatic H bonding) and π-Interaction (π-cation) interaction. The other information about the glide docking properties has been depicted in **Table 3.** The resultant docking bond distance and interaction type in ABuCP and 1,3-DNB **(Figure 15 and 16)** has been representing in **Table 4** and **Table 5.**

3.7. In-silico Complexation behavior:

The optimization of the complex (having hydrogen bonding interaction) has proceeded for two different types of docking poses, but at the end we are receiving the same optimization step **(Figure 17)** through which we had carried out our further studies. The optimization energy has been utilized for complexation behavior of ABuCP_1,3-DNB in both the gas well as solvent

phase at higher level of basis sets depicted in **(Table 6)** The binding energy (E_b) **(Table 7)** has been calculated using below equation:

$$E_b = E_C - (E_L + E_A) \qquad (2)$$

Where, E_r= complex (ABuCP_1,3-DNB) optimization energy (Hartree); E_L=ABuCP optimization energy (Hartree); E_A=Analyte (NACs) optimization energy (Hartree).

3.8. Other Molecular Properties:

Further study of the Frontier molecular orbital (FMOs) energy such as Higher occupied molecular orbital (HOMO) and Lowest Unoccupied molecular orbital (LUMO) energy and other molecular properties to understand the nature of complexation among ABuCP and 1,3-DNB was carried out. The investigation of other molecular properties involves Chemical reactivity [like Hardness and Softness] and electronic properties [like electron density (ED), electrostatic potential (ESP), and Molecular electrostatic potential (MEP)].

Exploration of the global electronic descript such as hardness (η), chemical potential (μ), and Softness (S) through the Frontier molecular orbital (FMOs) difference i.e. The energy difference between HOMO and LUMO is of utmost importance for detailed understanding of chemical selectivity and reactivity in the concept of DFT [58-61]. The molecule with a larger energy gap lacks the possibility to proceed the electron in excited state which indicates the relative higher stability of the molecule [62].

The band gap energy (E_g) is a critical factor for the stability [63], softness (S) [60], hardness (η) [58,64] and chemical potential (μ) has been calculated using below equations:

$$E_g = E_{HOMO} - E_{LUMO} \qquad (4)$$

$$\eta = \frac{E_{LUMO} - E_{HOMO}}{2} \qquad (5)$$

$$S = \frac{1}{2\eta} \qquad (6)$$

$$\mu = \frac{E_{HOMO} + E_{LUMO}}{2} \qquad (7)$$

Maximum hardness principle (MHP) suggests that the system in their ground or valence state would make all the possible efforts to arrange themselves to be as hard as possible [65].

Electrophilicity is yet another global index which is a crucial term for energy reduction due to the maximum current of the electron between donor and acceptor [63].

$$\omega = \frac{\mu^2}{2\eta} \qquad (8)$$

The stabilization energy (ΔE) calculated as follow:

$$\Delta E = -\frac{\mu^2}{2\eta} \qquad (9)$$

Table 8 represents the energy of HOMO and LUMO of ABuCP, 1,3-DNB, and ABuCP_1,3-DNB complexes. As per the results, the following point directs important chemistry through the global electronic descriptor (a) The direction of electron transfer has been determined through the Electron chemical potential (μ). Also, the chemical potential value of the 1,3-DNB (-6.092 a.u) is more electronegative compared to the ABuCP (-2.7285 a.u) Which directs the electron transfer from the occupied of the ABuCP_1,3-DNB complex is responsible for the stability of it. (b) The lower the electrophilicity value acts as donor. The electrophilicity value of 1,3-DNB is higher compared to the ABuCP, denotes the greater electrophilicity ABuCP due to electrophilicity changes in ABuCP_1,3-DNB utilized as an acceptor during the encapsulation process. (c) The global harness (η) of the ABuCP reduced after the complexation with 1,3-DNB. Therefore, the theoretical results predict that the charge transfer interaction has a mandate role for the stabilization of the complexation process.

Figure 18 represents the HOMO and LUMO diagram of ABuCP, 1,3-DNB and ABuCP_1,3-DNB complex in solvent phase which indicates the affluence of electron transfer from HOMO of ABuCP to LUMO of 1,3-DNB through solvent media. The TDDFT section delivers more outcomes on the electron transfer process.

The electrostatic potential (ESP) **(Figure 19, 20 and 21)** was higher slightly at hydroxy oxygen at carboxylic acid and Nitrogen in ABuCP. The Electron density (ED) **(Figure 19, 20 and 21)** has been uniformly distributed to ABuCP, 1,3-DNB as well as ABuCP_1,3-DNB complex. **Figure 21** represents that in the direction of the pyrrole ring more +ve potential is found and that the more negative potential is in the direction of the carboxylic group of butyric acid as well as 1,3-DNB compared to ABuCP and 1,3-DNB.

For the recognition and interaction of hydrogen bonding in complexation has been identified through Molecular electrostatic potential (MEP). In addition to these, MEP plays a vital role in predicting binding sites and relative relativities towards electrophilic and nucleophilic attack [66-68].

As per the **Figure 22, 23 and 24** the lone pair of the oxygen attached with Nitrogen in the -NO_2 group in 1,3-DNB forms a hydrogen bond with the hydrogen atom attached with pyrrole N-atom.

3.9. Time dependent density functional theory calculation:

To further evaluate the electron transfer and the mechanism, the Time dependent density functional theory (TD-DFT) was carried out in solvent phase (Methanol) for the first six excited states at the levels CAM-B3LYP with the 6-31G(d,p) basis set. In addition to this, TD-DFT was used to nitro aromatic compounds the UV-Vis absorption spectra of the ABuCP as well as ABuCP_1,3-DNB complex. **Table 9** represents the excitation energy (E), oscillator strength (f), wavelength (λ), key transition and the % contribution of the transition with their total energy which was compared with the experimental excitation energy. The frontier molecular orbitals (FMO's) and maximum wavelength absorption of ABuCP has been depicted in **Figure 25** and **Table 9.** The UV-Vis spectra were obtained due to the electron transition of HOMO (HOMO-1 and HOMO-3) to LUMO (LUMO-4, LUMO-6, and LUMO-7). Among all transitions, the % contribution of more than 15% of **HOMO→LUMO+7, HOMO-1→LUMO+4, HOMO→LUMO+6** were responsible for the UV-Vis spectra of ABuCP. The FMO's and maximum wavelength absorption of ABuCP_1,3-DNB complex was depicted in **Figure 26** and **Table 9.** Also transitions as **HOMO-12→LUMO+1, HOMO-10→LUMO+1** contribute more than 15% and they also contribute a key role for the development of the UV-Vis spectra of the ABuCP_1,3-DNB complex.

Practically, 24 nm red shift appeared in ABuCP_1,3-DNB complex in methanol solvent while the TDDFT study has a resemblance of about 30 nm red shift for the ABuCP_1,3-DNB complex in methanol as a solvent.

4.0. Conclusion

A unique and novel 1,3-DNB sensor has been designed and developed using ABuCP as host ligand. Additionally, ABuCP acts as a rapid, highly sensitive, and selective receptor towards 1,3-DNB. Molecular modelling studies favours the complexation behaviour of the synthesized host and guest. In addition, the Host-guest interaction analysis through in-silico method favors the complexation with 1,3-DNB via H-bonding and π- π interaction. Other molecular properties support the charge transfer from 1,3-DNB to ABuCP. The TDDFT support the charge transfer from HOMO→LUMO-7, HOMO-1→LUMO+4, HOMO-1→LUMO+6, HOMO-12→LUMO+1, HOMO-10→LUMO+1 transition with 24 nm red shift. Such sensing devices can be prepared from ABuCP to detect 1,3-DNB in a very low concentration range also. Also, its novel derivative; calix[4]pyrrole carrying anthraquinone i.e. ABuCPTAA has been successfully synthesized and characterized. Its complexation behavior with various metal ions is studied by absorption and emission spectroscopy. It exhibited high selectivity for Sr (II) ion with a good quenching. The binding studies were further supported by stoichiometric studies in which 1:1 binding was found. Also binding constant and limit of detection were calculated up to 10 μM. Further quantum yield was found for the same. In addition to Sr (II) ions the turn-off mechanism arises, the reason behind it is prohibition of charge transfer from oxygen of anthraquinone group to electron deficient ring.

Author Declarations

- ✓ Funding (information that explains whether and by whom the research was supported)
  This research received no external funding.
- ✓ Conflicts of interest/Competing interests (include appropriate disclosures)
  This research received no external funding.
- ✓ Ethics approval/declarations (include appropriate approvals or waivers)
  Not Applicable
- ✓ Consent to participate (include appropriate statements)
  Not Applicable
- ✓ Consent for publication (include appropriate statements)
  Not Applicable
- ✓ Availability of data and material/ Data availability (data transparency, if link please provide the link to access.
  No repository
- ✓ Code availability (software application or custom code)
  Not Applicable
- ✓ Authors' contributions (all authors should be individually mentioned in the author contribution statement.
  ALD Synthesized molecules and purified. NPP characterised and interpreted the data. JHP Wrote data in manuscript (Editor) form using structure software's. KMM analysed the application in silico using software. KDB major contributor in writing the manuscript and analysis the structural data

[LIST AUTHORS AND DATED SIGNATURES ALONGSIDE]

Name of Authors	Signature/Date
Mr. Ajay L. Desai (ALD)	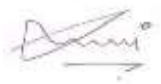 17-09-2021
Mr. Nihal P. Patel (NPP)	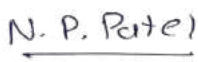 17-09-2021
Mr. Jaymin H. Parikh (JHP)	 17-09-2021
Dr. Krunal M. Modi (KMM)	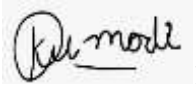 17-09-2021
Dr. Keyur D. Bhatt (KDB)	 17-09-2021

5.0. References

1. Senra, J. D., Malta, L. F. B., da Costa, M. E., Michel, R. C., Aguiar, L. C., Simas, A. B., et al. (2009). Hydroxypropyl-α-Cyclodextrin-Capped Palladium Nanoparticles: Active Scaffolds for Efficient Carbon-Carbon Bond Forming Cross-Couplings in Water. *Advanced Synthesis & Catalysis, 351*(14-15), 2411-2422.
2. Rouhi, A. M. (1997). Land Mines-Horrors Begging for Solutions. *Chemical & engineering news, 75*(10), 14-22.
3. Yinon, J. (2002). Field detection and monitoring of explosives. *TrAC Trends in Analytical Chemistry, 21*(4), 292-301.
4. Arshad, N., Janjua, N. K., Ahmed, S., Khan, A. Y., & Skibsted, L. H. (2009). Electrochemical investigations of antioxidant interactions with radical anion and dianion of 1, 3-dinitrobenzene. *Electrochimica Acta, 54*(26), 6184-6189.
5. Modi, K., Panchal, U., Patel, C., Bhatt, K., Dey, S., Mishra, D., et al. (2018). Dual in vitro and in silico analysis of thiacalix [4] arene dinaphthalene sulfonate for the sensing of 4-nitrotoluene and 2, 3-dinitrotoluene. *New Journal of Chemistry, 42*(4), 2682-2691.
6. Chen, B. B., Liu, Z. X., Zou, H. Y., & Huang, C. Z. (2016). Highly selective detection of 2, 4, 6-trinitrophenol by using newly developed terbium-doped blue carbon dots. *Analyst, 141*(9), 2676-2681.
7. Ma, Y., Li, H., Peng, S., & Wang, L. (2012). Highly selective and sensitive fluorescent paper sensor for nitroaromatic explosive detection. *Analytical chemistry, 84*(19), 8415-8421.
8. Kulkarni, M., & Chaudhari, A. (2007). Microbial remediation of nitro-aromatic compounds: an overview. *Journal of Environmental Management, 85*(2), 496-512.
9. Bähring, S., Root, H. D., Sessler, J. L., & Jeppesen, J. O. (2019). Tetrathiafulvalene-calix [4] pyrrole: a versatile synthetic receptor for electron-deficient planar and spherical guests. *Organic & biomolecular chemistry, 17*(10), 2594-2613.
10. Floriani, C. (1996). Transition metal complexes as bifunctional carriers of polar organometallics: Their application to large molecule modifications and to hydrocarbon activation. *Pure and applied chemistry, 68*(1), 1-8.
11. Steinberg, R. S., Nayak, A., O'Connell, C., Burford, S., Pekarek, A., Chesnut, N., et al. (2020). Sex differences in eligibility for advanced heart failure therapies. *Clin Transplant*, e13839, doi:10.1111/ctr.13839.
12. Frisch, M., Trucks, G., Schlegel, H., Scuseria, G., Robb, M., Cheeseman, J., et al. (2009). Gaussian 09, Revision D. 01, 2009, Gaussian. *Inc., Wallingford CT*.
13. Walsh, M. E. (2001). Determination of nitroaromatic, nitramine, and nitrate ester explosives in soil by gas chromatography and an electron capture detector. *Talanta, 54*(3), 427-438.

14. Bader, M., Göen, T., Müller, J., & Angerer, J. (1998). Analysis of nitroaromatic compounds in urine by gas chromatography–mass spectrometry for the biological monitoring of explosives. *Journal of Chromatography B: Biomedical Sciences and Applications, 710*(1-2), 91-99.
15. Khayamian, T., Tabrizchi, M., & Jafari, M. (2003). Analysis of 2, 4, 6-trinitrotoluene, pentaerythritol tetranitrate and cyclo-1, 3, 5-trimethylene-2, 4, 6-trinitramine using negative corona discharge ion mobility spectrometry. *Talanta, 59*(2), 327-333.
16. Jimenez, A., & Navas, M. (2004). Chemiluminescence detection systems for the analysis of explosives. *Journal of hazardous materials, 106*(1), 1-8.
17. Wang, D., Ivanova, L. V., Ivanov, M. V., Mirzaei, S., Timerghazin, Q. K., Reid, S. A., et al. (2018). An Electron-Rich Calix [4] Arene-Based Receptor With Unprecedented Binding Affinity For Nitric Oxide. *Chemistry*.
18. Hamzi, I., Fray, M., Abidi, R., & Barhoumi-Slimi, T. (2019). Synthesis, characterization and conformational study of new α, β-unsaturated acylhydrazones based on calix [4] arene backbone. *Journal of Molecular Structure, 1185*, 78-84.
19. Panchal, M., Kongor, A., Athar, M., Modi, K., Patel, C., Dey, S., et al. (2020). Structural motifs of oxacalix [4] arene for molecular recognition of nitroaromatic explosives: Experimental and computational investigations of host-guest complexes. *Journal of Molecular Liquids, 306*, 112809.
20. Park, J. S., Le Derf, F., Bejger, C. M., Lynch, V. M., Sessler, J. L., Nielsen, K. A., et al. (2010). Positive homotropic allosteric receptors for neutral guests: annulated tetrathiafulvalene–calix [4] pyrroles as colorimetric chemosensors for nitroaromatic explosives. *Chemistry–A European Journal, 16*(3), 848-854.
21. Zhu, W., Park, J. S., Sessler, J. L., & Gaitas, A. (2011). A colorimetric receptor combined with a microcantilever sensor for explosive vapor detection. *Applied Physics Letters, 98*(12), 123501.
22. Kim, D.-S., Lynch, V. M., Nielsen, K. A., Johnsen, C., Jeppesen, J. O., & Sessler, J. L. (2009). A chloride-anion insensitive colorimetric chemosensor for trinitrobenzene and picric acid. *Analytical and bioanalytical chemistry, 395*(2), 393-400.
23. Bhatt, K. D., Gupte, H. S., Makwana, B. A., Vyas, D. J., Maity, D., & Jain, V. K. (2012). Calix receptor edifice; scrupulous turn off fluorescent sensor for Fe (III), Co (II) and Cu (II). *Journal of fluorescence, 22*(6), 1493-1500.
24. Bhatt, K. D., Makwana, B. A., Vyas, D. J., Mishra, D. R., & Jain, V. K. (2014). Selective recognition by novel calix system: ICT based chemosensor for metal ions. *Journal of Luminescence, 146*, 450-457.
25. Bhatt, K. D., Shah, H. D., Modi, K. M., Narechania, M. B., & Patel, C. (2019). Calix [4] pyrrole virtuous sensor: a selective and sensitive recognition for Pb (II) ions by spectroscopic and computational study. *Supramolecular Chemistry, 31*(4), 268-282.

26. Bhatt, K. D., Vyas, D. J., Makwana, B. A., Darjee, S. M., Jain, V. K., & Shah, H. (2016). Turn-on fluorescence probe for selective detection of Hg (II) by calixpyrrole hydrazide reduced silver nanoparticle: Application to real water sample. *Chinese Chemical Letters, 27*(5), 731-737.
27. Kim, S. K., & Sessler, J. L. (2014). Calix [4] pyrrole-based ion pair receptors. *Accounts of chemical research, 47*(8), 2525-2536.
28. Lee, C.-H. (2011). Versatilities of calix [4] pyrrole based anion receptors. *Bulletin of the Korean Chemical Society, 32*(3), 768-778.
29. Matthews, S. E., & Beer, P. D. (2005). Calixarene-based anion receptors. *Supramolecular Chemistry, 17*(6), 411-435.
30. Schneider, H. J. (2009). Binding mechanisms in supramolecular complexes. *Angewandte Chemie International Edition, 48*(22), 3924-3977.
31. Wheate, N. J., Buck, D. P., Day, A. I., & Collins, J. G. (2006). Cucurbit [n] uril binding of platinum anticancer complexes. *Dalton transactions*(3), 451-458.
32. Mutihac, L., Buschmann, H.-J., Mutihac, R.-C., & Schollmeyer, E. (2005). Complexation and separation of amines, amino acids, and peptides by functionalized calix [n] arenes. *Journal of Inclusion Phenomena and Macrocyclic Chemistry, 51*(1-2), 1-10.
33. Lehn, J.-M. (2002). Toward self-organization and complex matter. *Science, 295*(5564), 2400-2403.
34. Paulini, R., Müller, K., & Diederich, F. (2005). Orthogonal multipolar interactions in structural chemistry and biology. *Angewandte Chemie International Edition, 44*(12), 1788-1805.
35. Kongor, A., Panchal, M., Athar, M., Makwana, B., Sindhav, G., Jha, P., et al. (2018). Synthesis and modeling of calix [4] pyrrole wrapped Au nanoprobe for specific detection of Pb (II): Antioxidant and radical scavenging efficiencies. *Journal of Photochemistry and Photobiology A: Chemistry, 364*, 801-810.
36. Panchal, M., Athar, M., Jha, P., Kongor, A., Mehta, V., Bhatt, K., et al. (2016). Turn-off fluorescence probe for the selective determination of pendimethalin using a mechanistic docking model of novel oxacalix [4] arene. *RSC advances, 6*(58), 53573-53577.
37. Darjee, S. M., Bhatt, K., Kongor, A., Panchal, M. K., & Jain, V. K. (2017). Thiacalix [4] arene functionalized gold nano-assembly for recognition of isoleucine in aqueous solution and its antioxidant study. *Chemical Physics Letters, 667*, 137-145.
38. Linn, M. M., Poncio, D. C., & Machado, V. G. (2007). An anionic chromogenic sensor based on the competition between the anion and a merocyanine solvatochromic dye for calix [4] pyrrole as a receptor site. *Tetrahedron letters, 48*(26), 4547-4551.
39. Kaur, S., Hwang, H., Lee, J. T., & Lee, C.-H. (2013). Displacement-based, chromogenic calix [4] pyrrole–indicator complex for selective sensing of pyrophosphate anion. *Tetrahedron letters, 54*(29), 3744-3747.
40. Suksai, C., & Tuntulani, T. (2003). Chromogenic anion sensors. *Chemical Society Reviews, 32*(4), 192-202.

41. Farinha, A. S., Fernandes, M. R., & Tomé, A. C. (2014). Chromogenic anion molecular probes based on β, β'-disubstituted calix [4] pyrroles. *Sensors and Actuators B: Chemical, 200*, 332-338.
42. Bhatt, K. D., Shah, H. D., & Panchal, M. (2017). A switch-off fluorescence probe towards Pb (II) and cu (II) ions based on a calix [4] pyrrole bearing amino-quinoline group. *Luminescence, 32*(8), 1398-1404.
43. Becke, A. D. (1988). Density-functional exchange-energy approximation with correct asymptotic behavior. *Physical review A, 38*(6), 3098.
44. Frisch, M., Trucks, G., Schlegel, H., Scuseria, G., Robb, M., Cheeseman, J., et al. (2016). Gaussian 16 Rev. B. 01, Wallingford, CT.
45. Frisch, M., Trucks, G., Schlegel, H., Scuseria, G., Robb, M., Cheeseman, J., et al. (2013). Gaussian 09 Rev. A. 02. Wallingford: Gaussian. Inc.
46. Hanwell, M. D., Curtis, D. E., Lonie, D. C., Vandermeersch, T., Zurek, E., & Hutchison, G. R. (2012). Avogadro: an advanced semantic chemical editor, visualization, and analysis platform. *Journal of cheminformatics, 4*(1), 1-17.
47. Friesner, R. A., Murphy, R. B., Repasky, M. P., Frye, L. L., Greenwood, J. R., Halgren, T. A., et al. (2006). Extra precision glide: Docking and scoring incorporating a model of hydrophobic enclosure for protein− ligand complexes. *Journal of medicinal chemistry, 49*(21), 6177-6196.
48. Friesner, R. A., Banks, J. L., Murphy, R. B., Halgren, T. A., Klicic, J. J., Mainz, D. T., et al. (2004). Glide: a new approach for rapid, accurate docking and scoring. 1. Method and assessment of docking accuracy. *Journal of medicinal chemistry, 47*(7), 1739-1749.
49. Bowers, K. J., Chow, D. E., Xu, H., Dror, R. O., Eastwood, M. P., Gregersen, B. A., et al. Scalable algorithms for molecular dynamics simulations on commodity clusters. In *SC'06: Proceedings of the 2006 ACM/IEEE Conference on Supercomputing, 2006* (pp. 43-43): IEEE
50. Blanchard, D. J., & Manderville, R. A. (2016). An internal charge transfer-DNA platform for fluorescence sensing of divalent metal ions. *Chemical Communications, 52*(61), 9586-9588.
51. VORA, M., KONGOR, A., PANCHAL, M., ATHAR, M., VERMA, A., PANJWANI, F., et al. (2020). A highly selective anthraquinone appended oxacalixarene receptor for fluorescent ICT sensing of F− ions: an experimental and computational study. *Journal of Chemical Sciences, 132*(1), 1-10.
52. Darjee, S. M., Modi, K. M., Panchal, U., Patel, C., & Jain, V. K. (2017). Highly selective and sensitive fluorescent sensor: Thiacalix [4] arene-1-naphthalene carboxylate for Zn2+ ions. *Journal of Molecular Structure, 1133*, 1-8.
53. Tedesco, A., Oliveira, D., Lacava, Z., Azevedo, R., Lima, E., & Morais, P. (2004). Investigation of the binding constant and stoichiometry of biocompatible cobalt ferrite-based magnetic fluids to serum albumin. *Journal of magnetism and magnetic materials, 272*, 2404-2405.

54. Patra, S., & Paul, P. (2009). Synthesis, characterization, electrochemistry and ion-binding studies of ruthenium (II) bipyridine receptor molecules containing calix [4] arene-azacrown as ionophore. *Dalton Transactions*(40), 8683-8695.
55. Sortino, S., Petralia, S., Pignataro, B., Marletta, G., Conoci, S., & Valli, L. (2003). Langmuir–Schäfer films of a new calix [4] pyrrole-based macrocycle exhibiting induced chirality upon binding with chiral alcohol vapours. *New Journal of Chemistry, 27*(3), 615-618.
56. Lee, J. Y., Root, H. D., Ali, R., An, W., Lynch, V. M., Bähring, S., et al. (2020). Ratiometric turn-on fluorophore displacement ensembles for nitroaromatic explosives detection. *Journal of the American Chemical Society, 142*(46), 19579-19587.
57. Liu, K., He, L., He, X., Guo, Y., Shao, S., & Jiang, S. (2007). Calix [4] pyrrole–TCBQ assembly: a signal magnifier of TCBQ for colorimetric determining amino acids and amines. *Tetrahedron Letters, 48*(24), 4275-4279.
58. Houk, K. N. (1975). Frontier molecular orbital theory of cycloaddition reactions. *Accounts of Chemical Research, 8*(11), 361-369.
59. Kohn, W., Becke, A. D., & Parr, R. G. (1996). Density functional theory of electronic structure. *The Journal of Physical Chemistry, 100*(31), 12974-12980.
60. Dizaji, N. J., Nouri, A., Zahedi, E., Musavi, S. M., & Nouri, A. (2017). Regioselectivity of 1, 3-dipolar cycloadditions between aryl azides and an electron-deficient alkyne through DFT reactivity descriptors. *Research on Chemical Intermediates, 43*(2), 767-782.
61. Fakhari, S., Nouri, A., Jamzad, M., Arab-Salmanabadi, S., & Falaki, F. (2021). Investigation of inclusion complex of metformin into selective cyclic peptides as novel drug delivery system: Structure, electronic properties, AIM, and NBO study via DFT. *Journal of the Chinese Chemical Society, 68*(1), 67-75.
62. Suvitha, A., Venkataramanan, N. S., Mizuseki, H., Kawazoe, Y., & Ohuchi, N. (2010). Theoretical insights into the formation, structure, and electronic properties of anticancer oxaliplatin drug and cucurbit [n] urils n= 5 to 8. *Journal of Inclusion Phenomena and Macrocyclic Chemistry, 66*(3), 213-218.
63. Koopmans, T. (1934). Über die Zuordnung von Wellenfunktionen und Eigenwerten zu den einzelnen Elektronen eines Atoms. *physica, 1*(1-6), 104-113.
64. Pearson, R. G. (2005). Chemical hardness and density functional theory. *Journal of Chemical Sciences, 117*(5), 369-377.
65. Scrocco, E., & Tomasi, J. (1978). Electronic molecular structure, reactivity and intermolecular forces: an euristic interpretation by means of electrostatic molecular potentials. In *Advances in quantum chemistry* (Vol. 11, pp. 115-193): Elsevier.
66. Luque, F. J., López, J. M., & Orozco, M. (2000). Perspective on "Electrostatic interactions of a solute with a continuum. A direct utilization of ab initio molecular potentials for the prevision of solvent effects". *Theoretical Chemistry Accounts, 103*(3), 343-345.

67. Okulik, N., & Jubert, A. H. (2005). Theoretical analysis of the reactive sites of non-steroidal anti-inflammatory drugs. *Internet Electronic Journal of Molecular Design, 4*(1), 17-30.

68. Miyaji, H., Kim, H.-K., Sim, E.-K., Lee, C.-K., Cho, W.-S., Sessler, J. L., et al. (2005). Coumarin-strapped calix [4] pyrrole: a fluorogenic anion receptor modulated by cation and anion binding. *Journal of the American Chemical Society, 127*(36), 12510-12512.

Figures

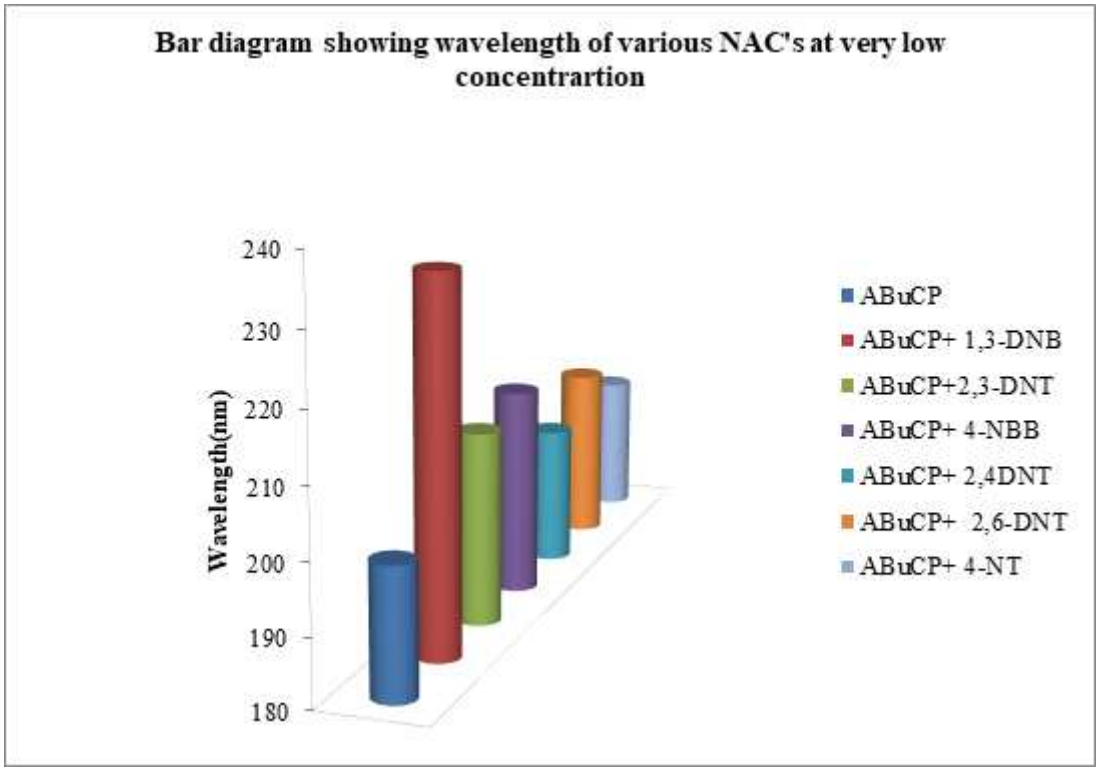

Figure 1

Bar diagram showing wavelength vs absorption of various explosives + ABuCP at very low concentration

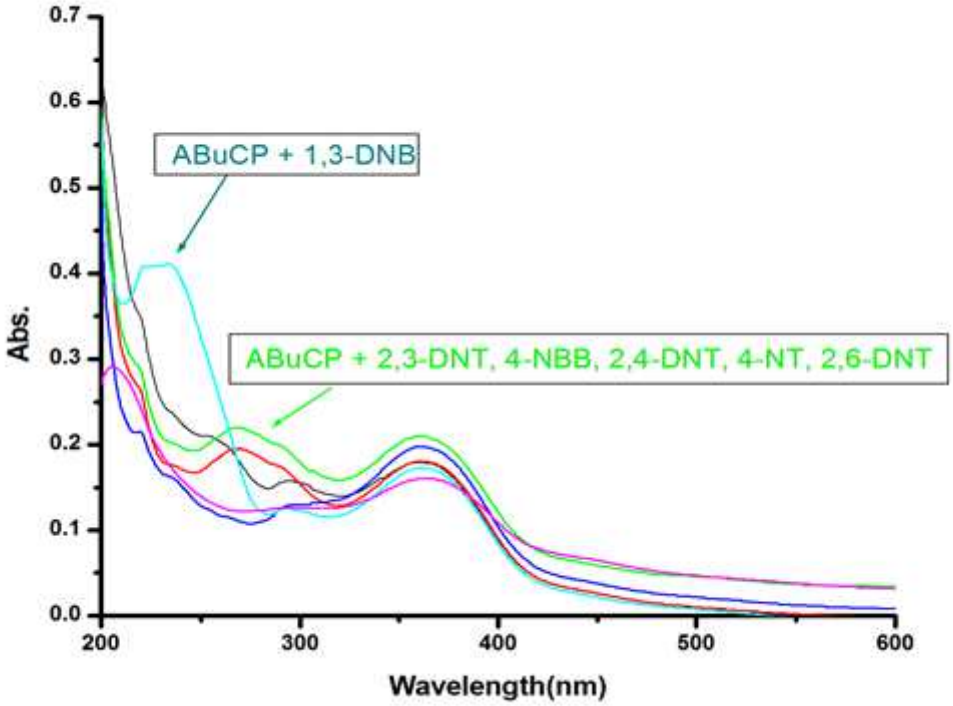

Figure 2

UV-vis response of the ABuCP (2 × 10-5mol L-1) towards the addition of explosives (2 × 10-5mol L-1) in methanol

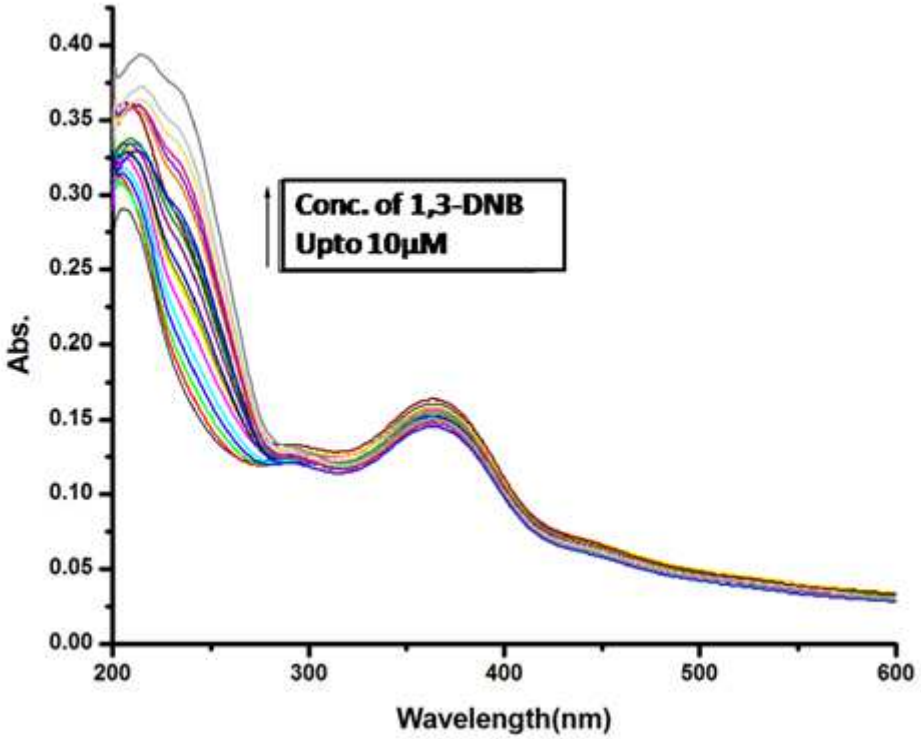

Figure 3

Variation of absorption intensity as well as wavelength upon the addition of gradually increasing concentration of 1,3-DNB

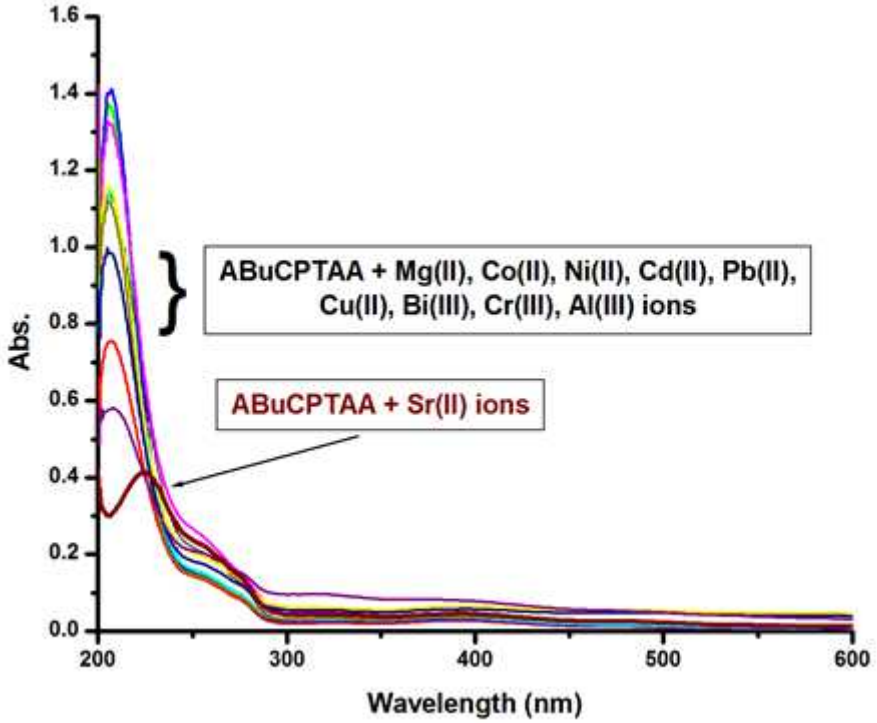

Figure 4

UV-Vis spectra of the ABuCPTAA (2 × 10-5 mol L-1) towards the addition of various metal ions (2 × 10-5 mol L-1) in methanol

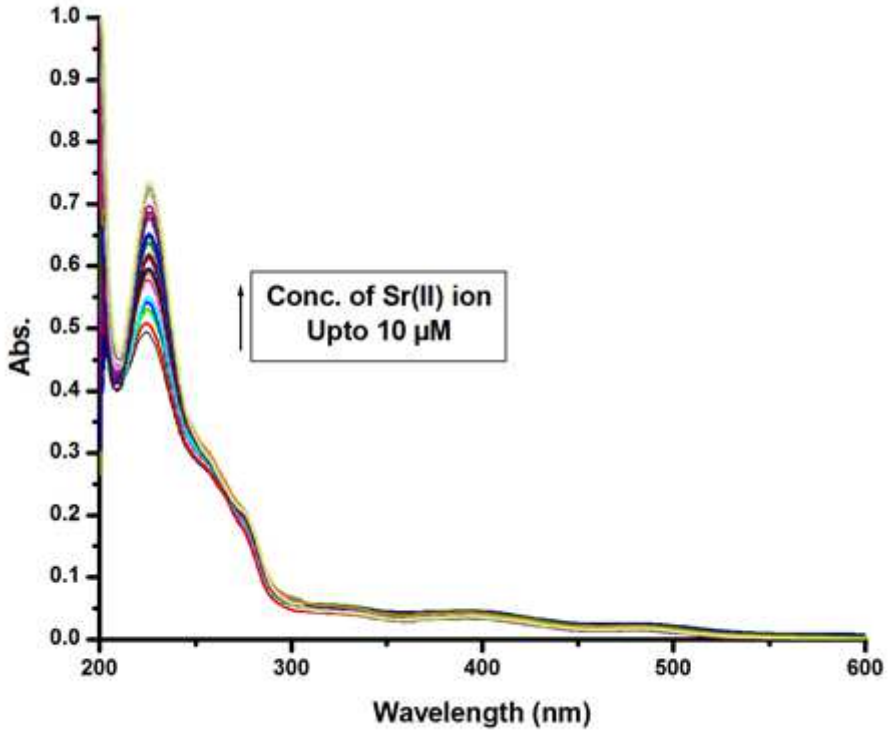

Figure 5

Variation of absorption intensity as well as wavelength upon the addition of gradually increasing concentration of Sr (II)

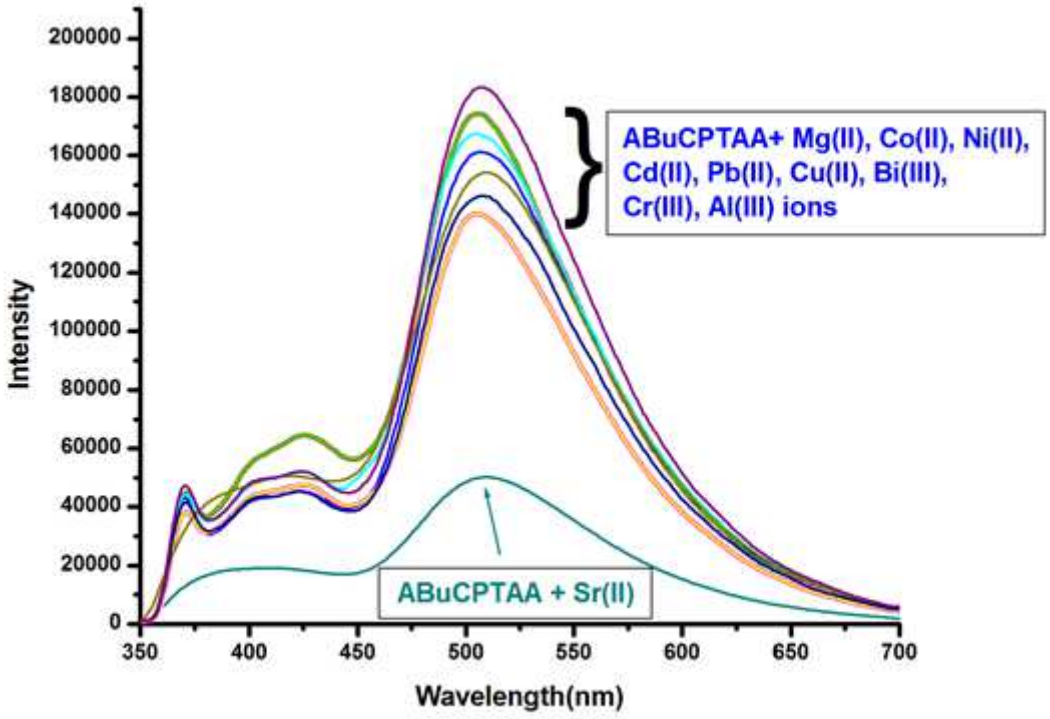

Figure 6

The fluorescence spectra of the ABuCPTAA (2 × 10-5 mol L-1) upon addition of various metal ions (2 × 10-5 mol L-1) in methanol

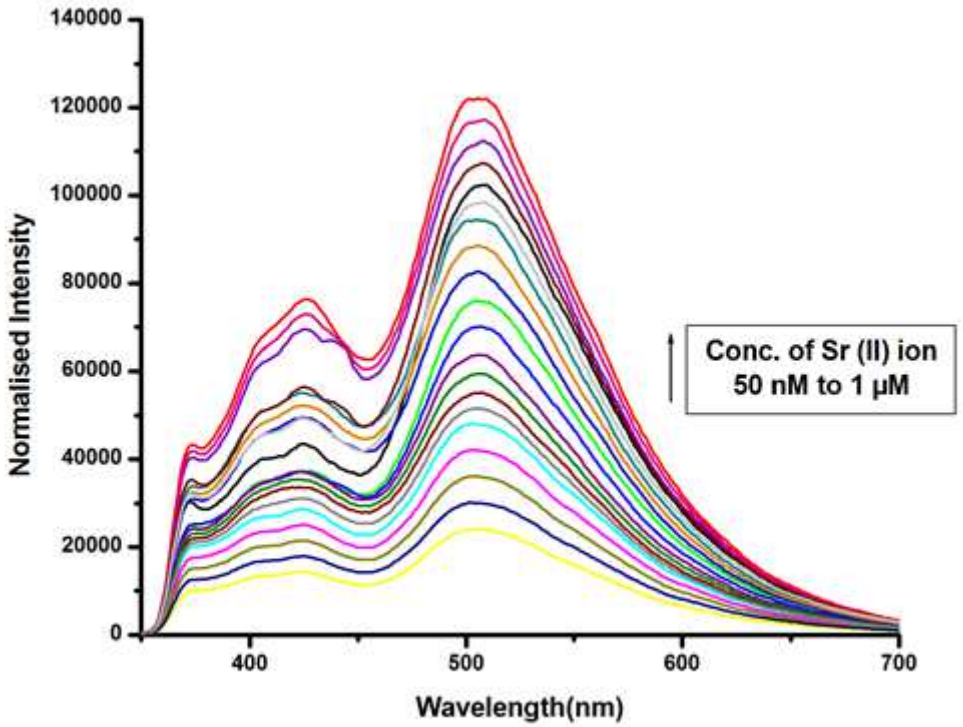

Figure 7

The fluorescence spectra of the ABuCPTAA (2 × 10-5 mol L-1) upon addition of 0-100 equivalents of Sr (II) in methanol

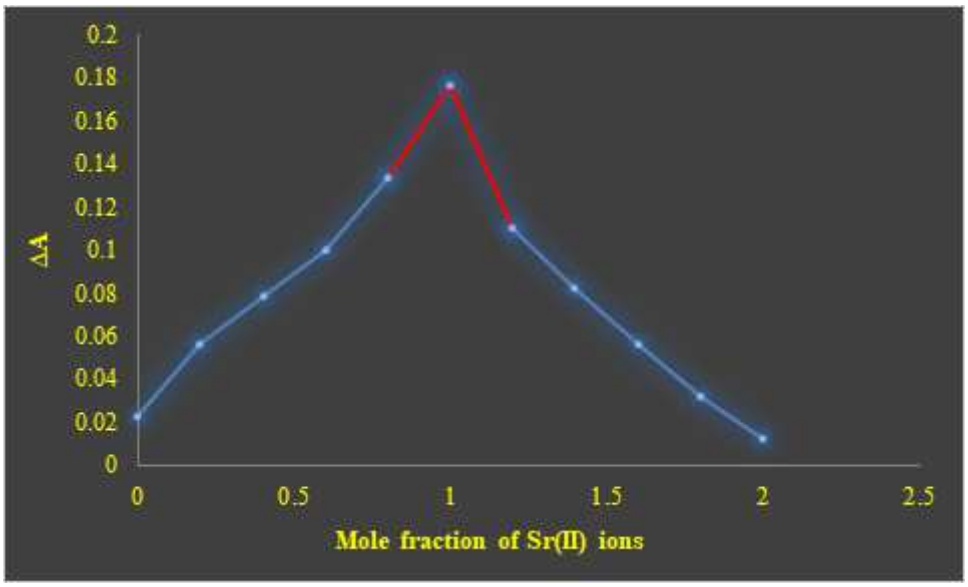

Figure 8

Job's plot of ABuCPTAA (2 × 10-5 mol L-1) with Sr (II) ions in MeOH

Figure 9

Colorimetric response of ABuCP towards various nitro aromatic compounds

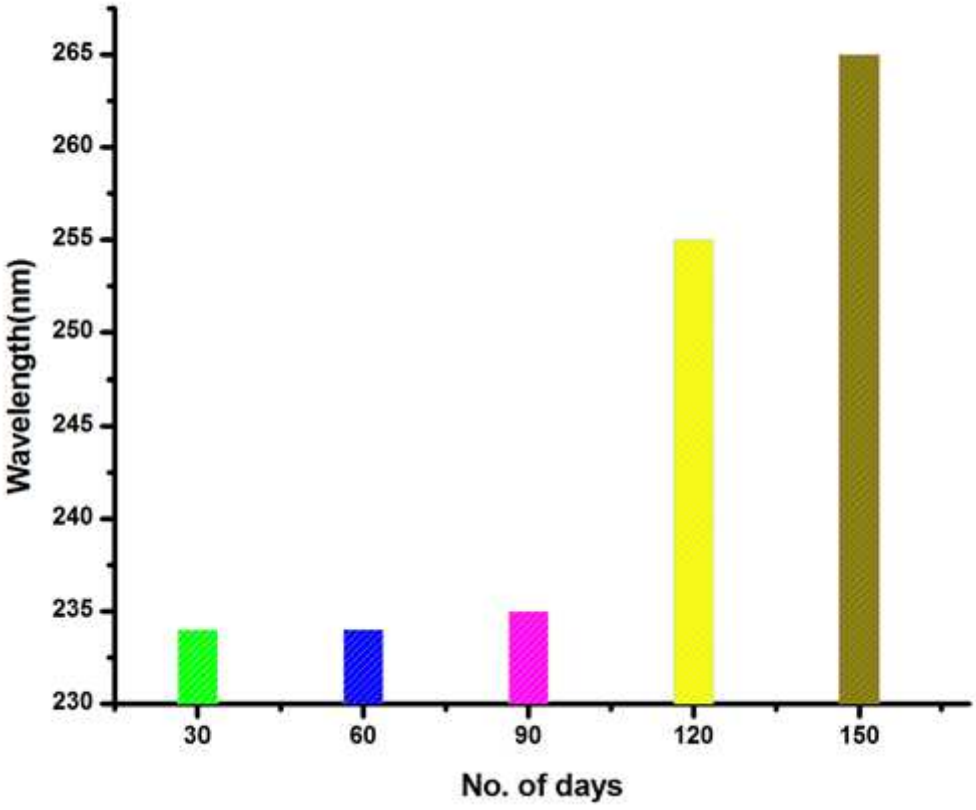

Figure 10

Stability study of ABuCP

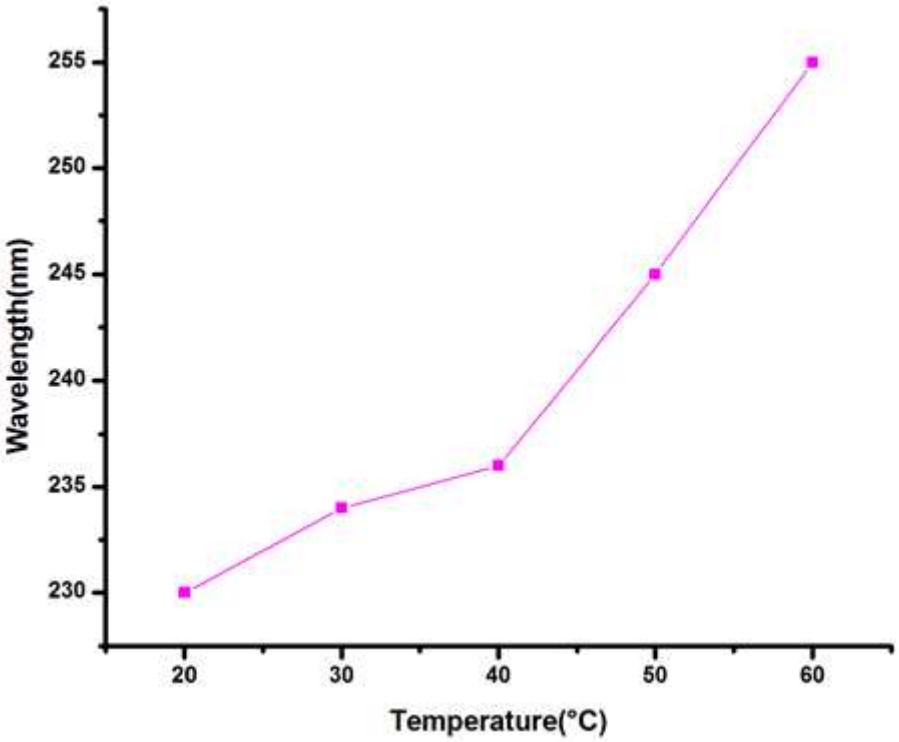

Figure 11

Temperature study of ABuCP

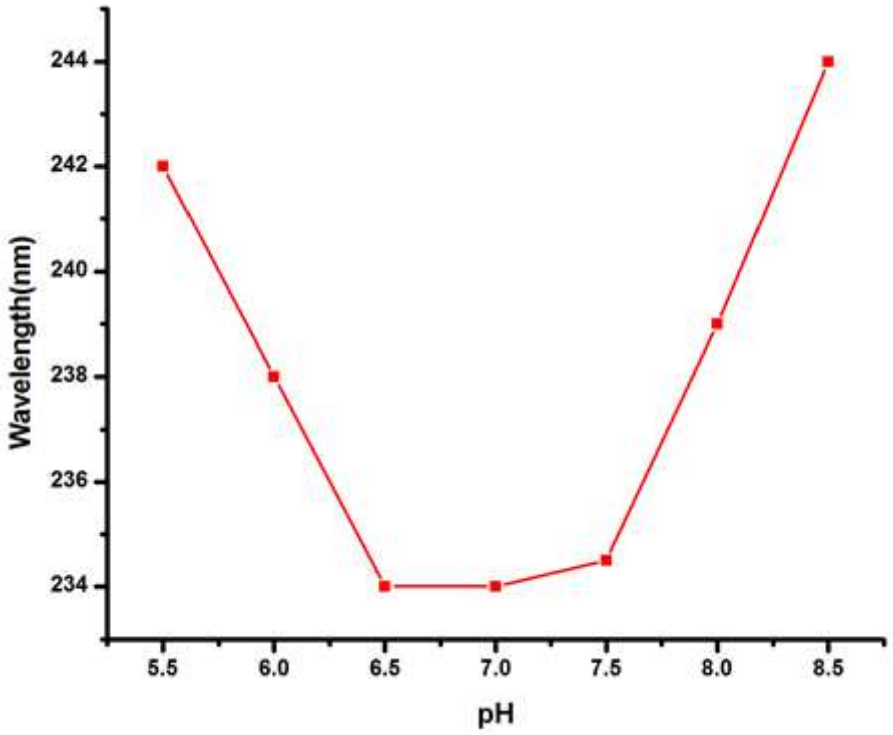

Figure 12

pH study of ABuCP

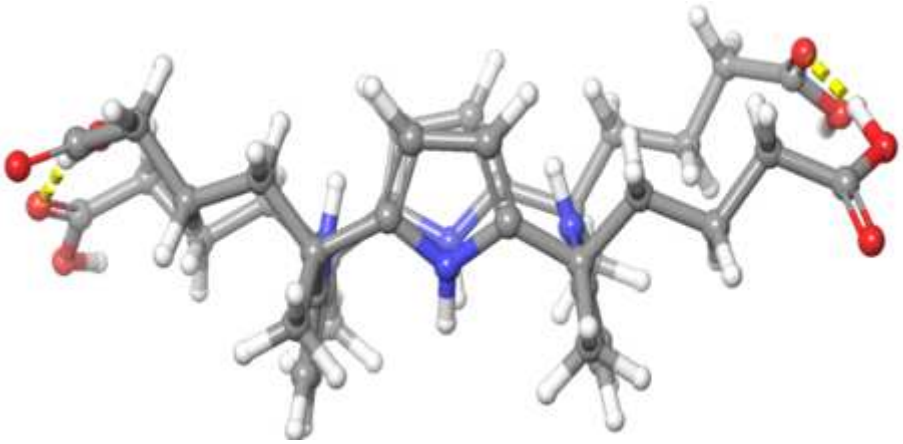

Figure 13

Geometry Optimization of ABuCP at b3lyp/6-31g(d,p) & cam- at b3lyp/6-31g(d,p) basis sets

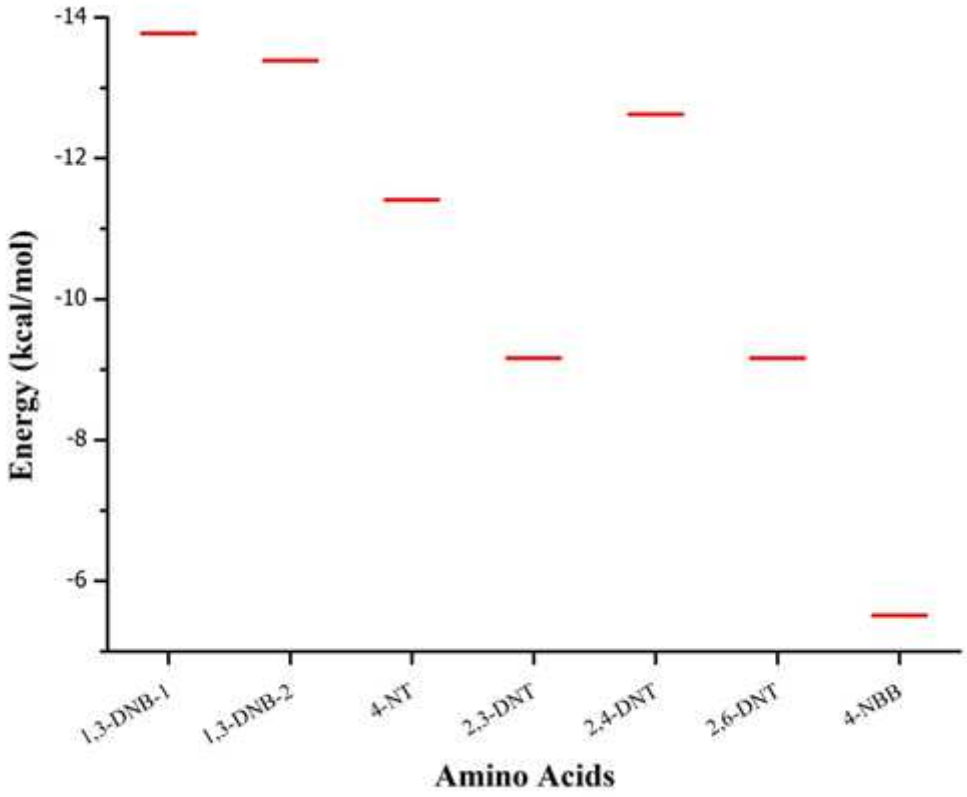

Figure 14

Glide docking energy for ABuCP (Host) with explosives (Guest)

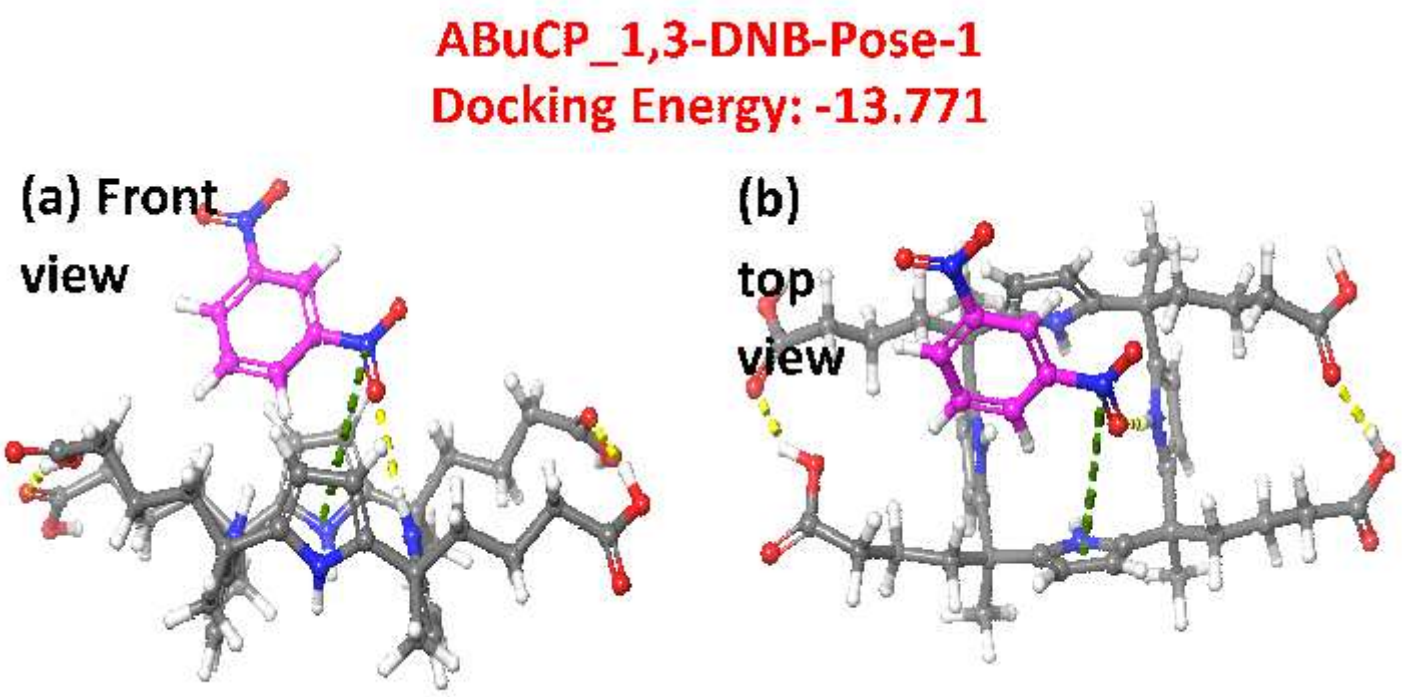

Figure 15

Docking poses of ABuCP_1,3-DNB 1,3-DNB complex-pose-1 (a) Front view; (b) top view (green color indicate the π-cation interaction and yellow color indicate Hydrogen bonding)

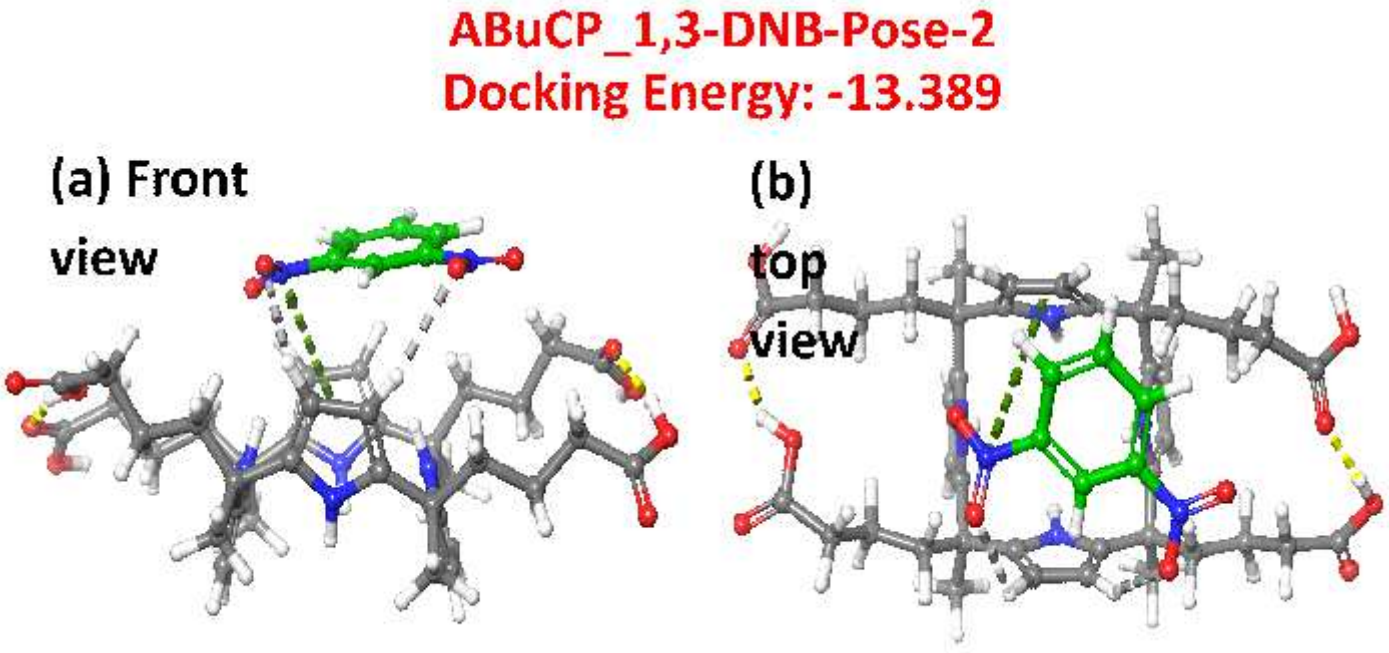

Figure 16

Docking poses of ABuCP_1,3-DNB complex-pose-2 (a) Front view; (b) top view (green color indicate the π-cation interaction and gray color indicate Aromatic Hydrogen bonding)

Figure 17

Optimization pose of docked pose-1 and pose-2 at Cam-B3LYP [6-31q(d,p)]

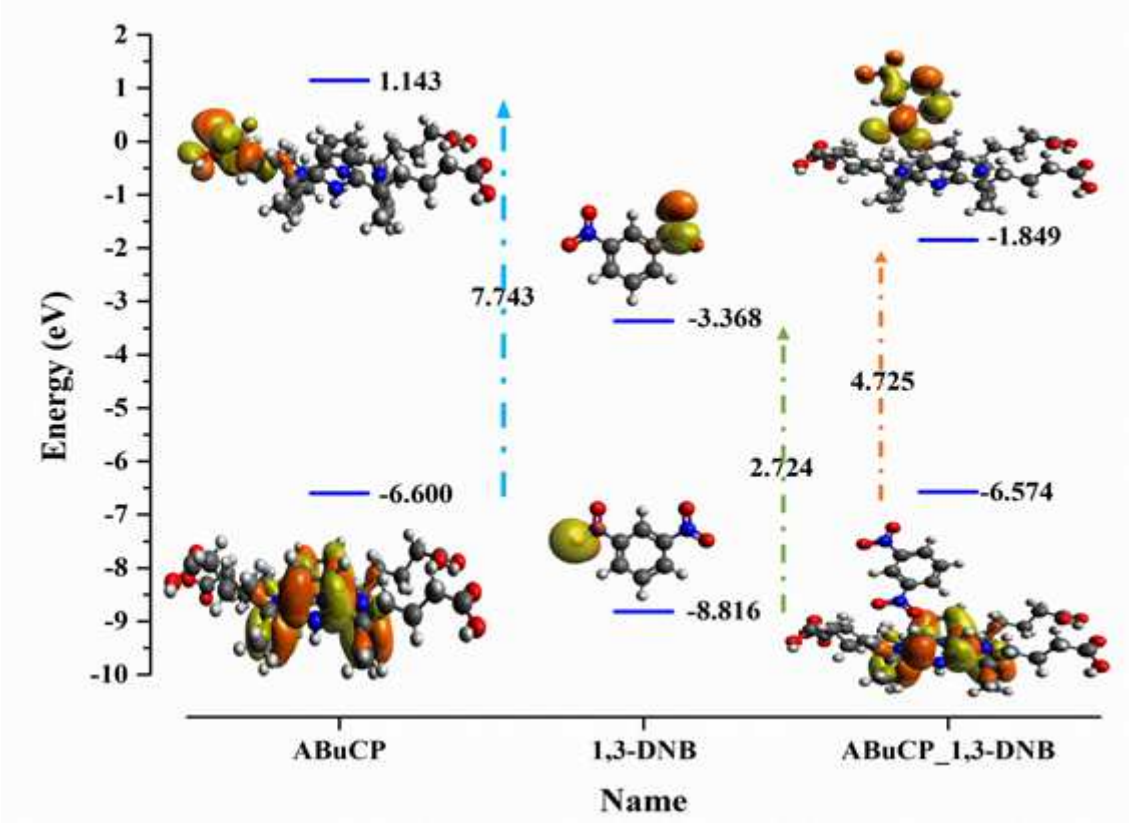

Figure 18

HOMO-LUMO energy diagram

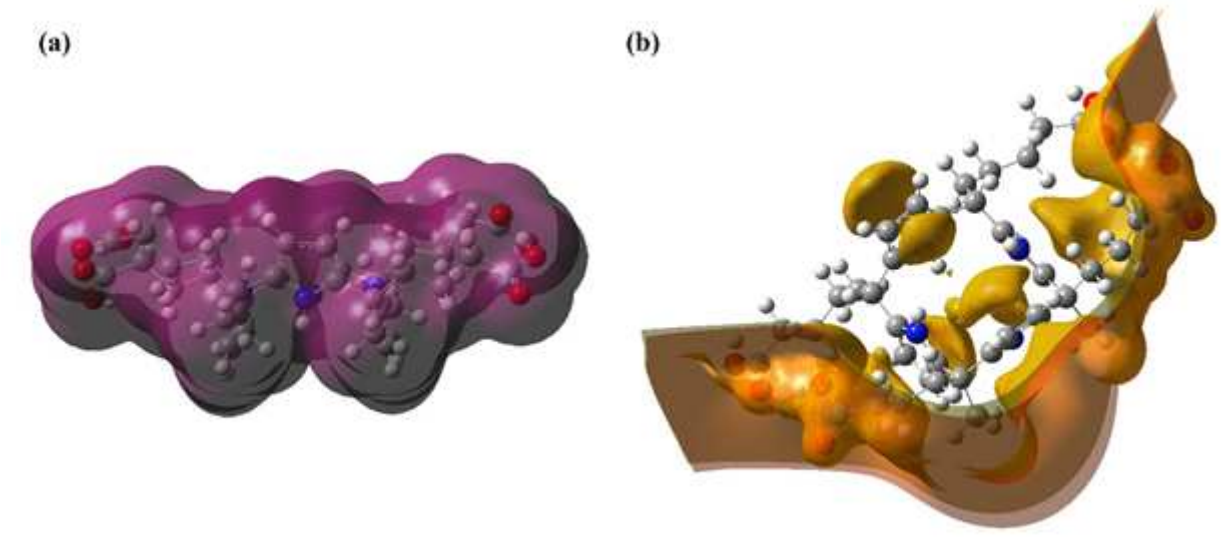

Figure 19

Other Molecular Properties of ABuCP (a) electron density (ED); (b) electrostatic potential (ESP)

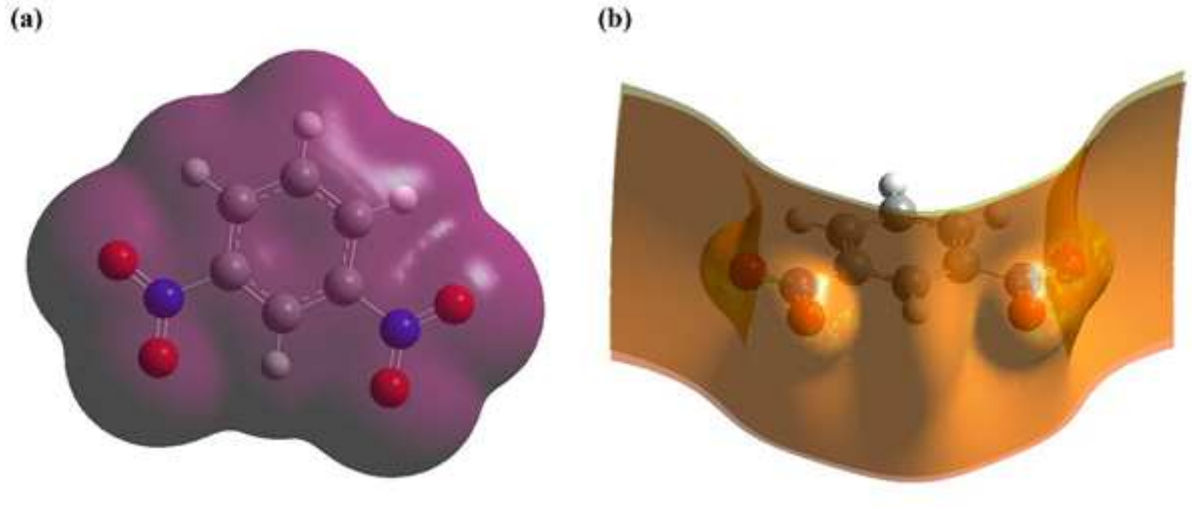

Figure 20

Other Molecular Properties of 1,3-DNB (a) electron density (ED); (b) electrostatic potential (ESP)

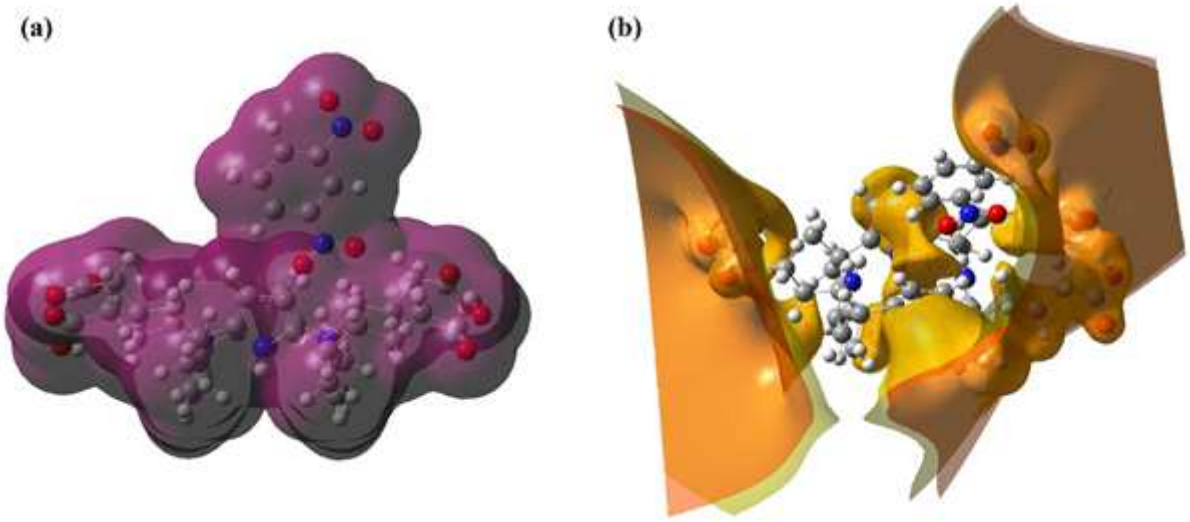

Figure 21

Other Molecular Properties of ABuCP_1,3-DNB complex (a) electron density (ED); (b) electrostatic potential (ESP)

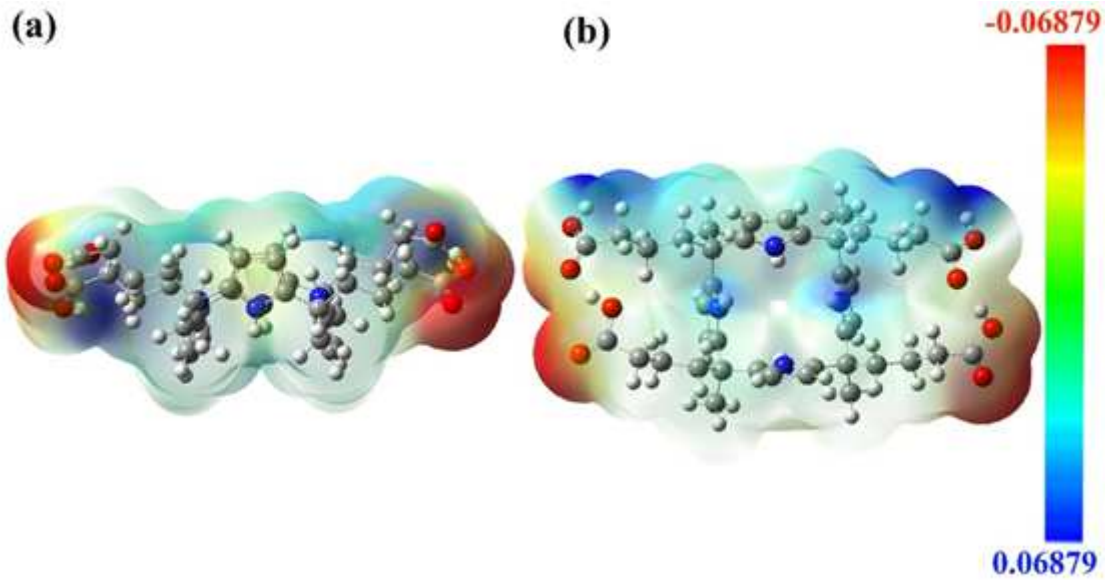

Figure 22

ABuCP molecular electrostatic potential (a) Front view; (b) top view

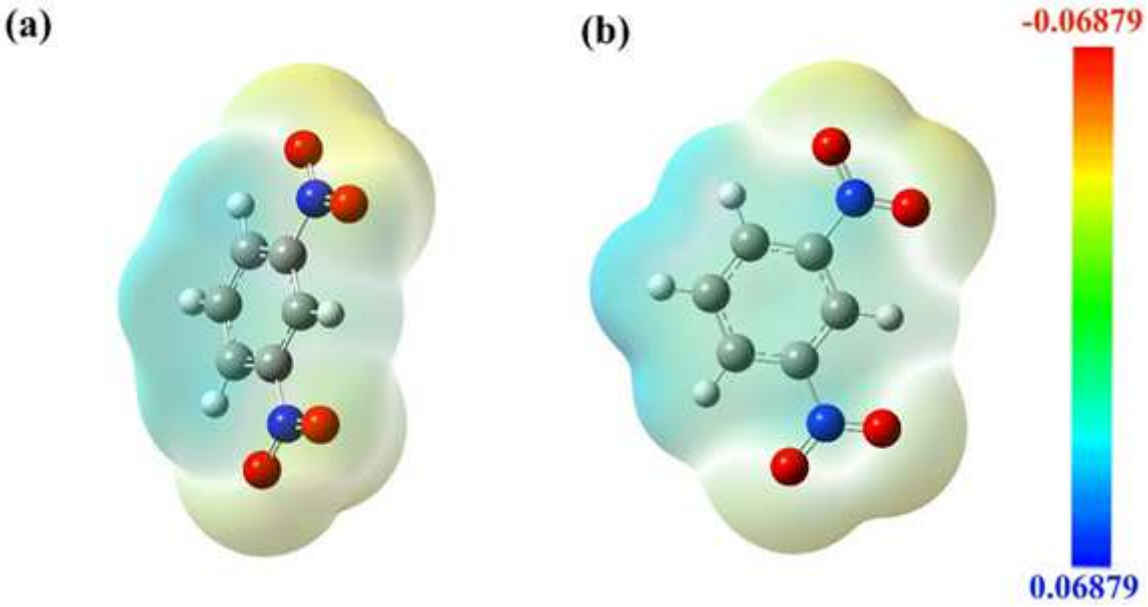

Figure 23

1,3-DNB molecular electrostatic potential (a) Front view; (b) top view

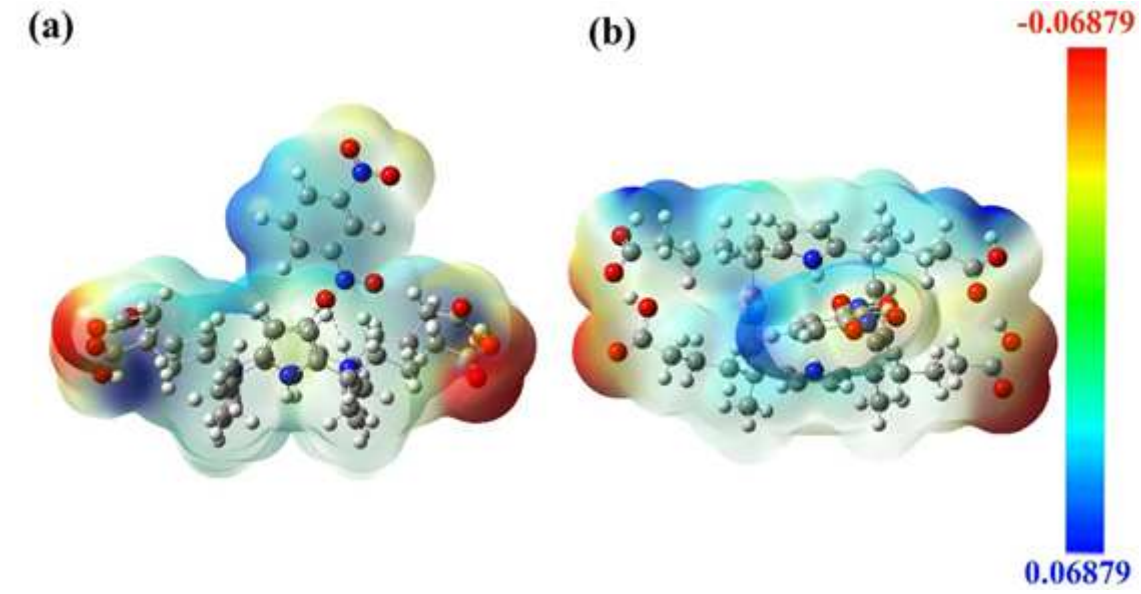

Figure 24

ABuCP_1,3-DNB molecular electrostatic potential (a) Front view; (b) top view

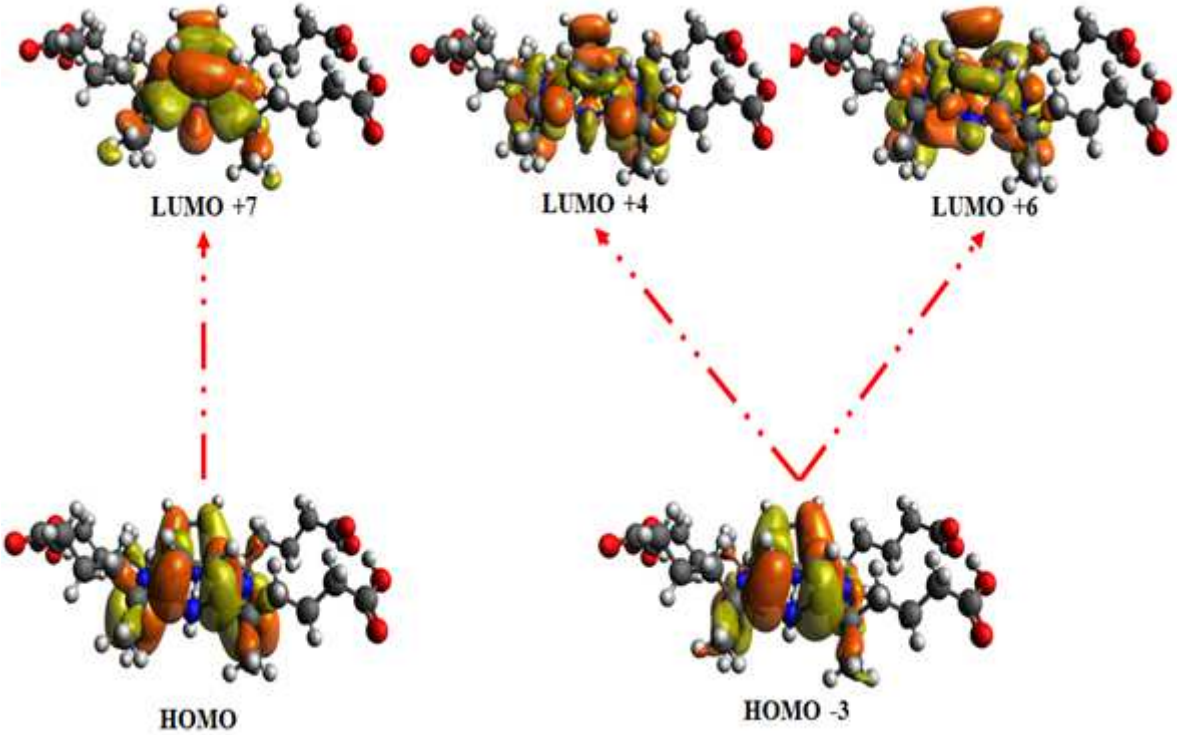

Figure 25

ABuCP Molecular orbital representation obtained at wavelength 199 nm (Practically 210 nm) through CPCM-TD- b3lyp/6-31g(d,p) level of approximation

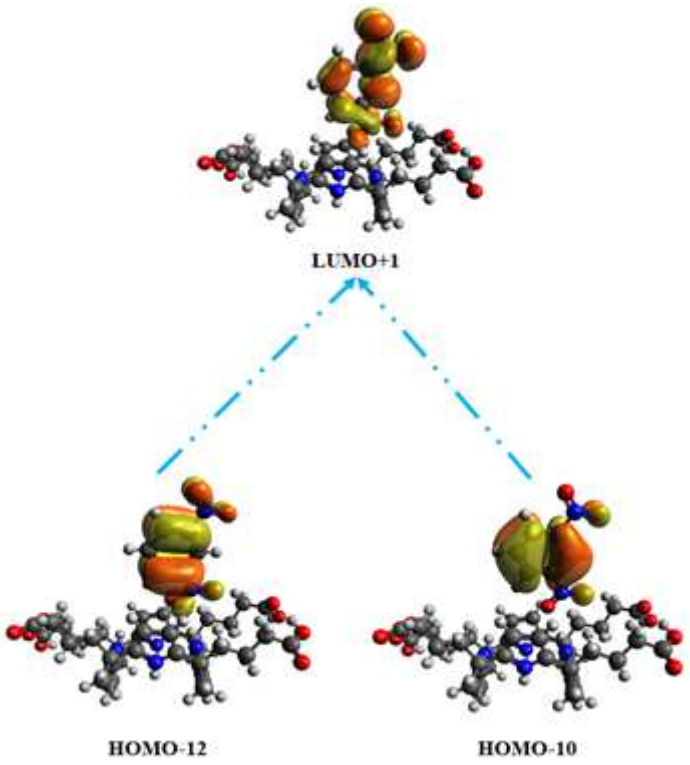

Figure 26

ABuCP _1,3-DNB Molecular orbital representation obtained at wavelength 230 nm (Practically 232 nm) through CPCM-TD- b3lyp/6-31g(d,p) level of approximation

Supplementary Files

This is a list of supplementary files associated with this preprint. Click to download.

- S1.png
- S2.png
- GraphicalAbstract.docx